Buoyancy-driven Thermal and Flow Characteristics in Gaps between Two Glasses of Multi-framed Window

JUHEE LEE

Department of ICT automotive engineering, Hoseo university, Dangjin, KOREA,
juheelee@hoseo.edu http://www.hoseo.ac.kr
YOUNJUN LEE
BEL technology, KOREA
leeyj@beltec.co.kr

Abstract: In building industry, both the beauty of the building facades and cost-effectiveness of the building are critical to occupants. The occupants long for the building that is more beautiful as well as comfort with low cost. For the beautiful facade, the more glasses are used and sometimes, the building covered with glasses. However, no glasses can prevent the heat energy flows out completely. Under the circumstance, to prevent the energy leakage through the window glass, multiple-framed windows are employed in architectural engineering in Korea. The gap between glasses is inevitable and the buoyancy-driven air flow in the gap between window glasses is one critical key for the heat transfer through the window. A numerical program for the air flow in the gap is developed considering gravity (buoyancy-driven momentum). Both the energy based on the temperature and the incompressible Navier-Stokes equations by using Boussinesq assumption are employed. A finite volume method based on the second-order accuracy is used to discretize, and a SIMPLE algorithm is employed to solve the pressure field instead of a decoupled continuity equation. The numerical validations are performed, and the reliability of the method is assessed. The characteristics of heat transfer and flow in three gaps are closely investigated with the developed code.

Key-Words: - Natural convection, Buoyancy-driven flow, Multi-framed window, Computational methods

1 Introduction

Windows consists of frame and glasses. To prevent energy leakage through the windows, multi-layered glasses with insulation liquid between them are used. One of the methods for energy saving is multiple framed windows that have two or three multi-layered glasses in a row. The air cavity between frames that add the complexities of design and engineering inevitably exists. The key of the heat transfer in the air cavity is a natural convection. Heat transfer by the natural convection is of interest in many industrial and architectural applications. The use of unstructured meshes for computation has become general because of geometrical complexity in the engineering problems.

The ability of unstructured meshes to discretize arbitrary and complex domains, the ease of local, and adaptive grid refinement which enhances the efficiency of the solution as well as accuracy are critical for the success of the numerical analysis. Among the discretization methods, the finite volume methods (FVM) are widely used for computational fluid dynamics (CFD). This is mainly due to the inherent conservativeness of FVM and ease of understanding. These FVMs are capable to accommodate arbitrary polyhedral grids composed of cells of various topologies. FVM is employed in this study calculating temperature and velocity field in an enclosed cavity.

Recently, Lestari [1] developed a numerical code for incompressible Navier-Stokes flow on triangular unstructured grids. A fully-implicit, Crank-Nicolson and an explicit four-step Runge-Kutta methods are used. The numerical algorithm used to solve the final equations is derived from the SIMPLER algorithm and four-stage Runge-Kutta to update the velocities directly without a pressure correction equation in addition to fully implicit and Crank-Nicholson methods.

Mathur and Murthy [2] have developed a pressure-based finite-volume method for the unstructured grid system. The method includes arbitrary polyhedral meshes, including meshes with non-conformal nodes. Cell-based, collocated storage is used. The high-order fluxes as well as secondary diffusion terms are computed using linear reconstruction and limiting similar to methods used for compressible flows. To minimize storage requirements, a segregated solution strategy is used, and SIMPLE algorithm is employed for pressure

and velocity coupled. An algebraic multigrid solver is used for the solution of linearized equations.

A single numerical code is not fully satisfied the all of the requirements in industrial purpose and thus, a lot of CFD program have been developed commercially [3, 4] and for research purpose. The flow in the cavity is laminar but is unstable because of its dimension (up to a few meters). The research on the flow and heat transfer is strongly required. Developing a CFD code based on the authors' previous study [5, 6] to calculate the natural convection phenomena next to the window cavity and window frame, we have been implementing a numerical code based on the SIMPLE method for solving three-dimensional incompressible flow using unstructured grids. In this study, flow and temperature according to window air cavity (gap) between frames will be carefully investigated, after validation of the flow field in an incompressible flow with a rectangular cavity. The mesh dependency test is also performed.

2 Numerical Methods

In the derivation of the governing equations of fluid dynamics, the Eulerian methods, spatially fixed control volume, is employed instead of Lagrangian methods. The laminar flow of an incompressible Newtonian fluid is assumed. The details can be found in Ref 5.

2.1 Finite volume methods

The equations for the transport of a scalar variable can be written in the following form:

$$\frac{\partial}{\partial t}\int_V \rho\phi dV + \int_S \left[\rho\phi\vec{v} - \Gamma_\phi\vec{\nabla}\phi\right]\cdot d\vec{S}$$
$$= \int_V Q_{\phi,V}dV + \int_S \vec{Q}_{\phi,S}\cdot d\vec{S} \qquad (1)$$

where ϕ, ε_ϕ, $Q_{\phi,S}$, and $Q_{\phi,V}$ stand for the transported variable, the diffusion coefficient, the surface exchange terms and volume sources, respectively. The momentum and energy equations can also be written in the form of (1) except an additional diffusion terms in the momentum equation.

The conservation equation of the continuity equation, for a control volume drive from the (1) implies that the rate of change of the mass inside the control volume is equal to the difference between inflow and outflow mass fluxes across the volume surface. In integral form, the continuity equation can be written as follows:

$$\frac{\partial}{\partial t}\int_V \rho dV + \int_S \left[\rho\vec{v}\right]\cdot d\vec{S} = 0 \qquad (2)$$

where, ρ is the fluid density and is the velocity. In incompressible flow, the first term in (2) is zero and the convection term cannot be ignored. More details including discretization, pressure correction and SIMPLE methods can be found in Ref. 7.
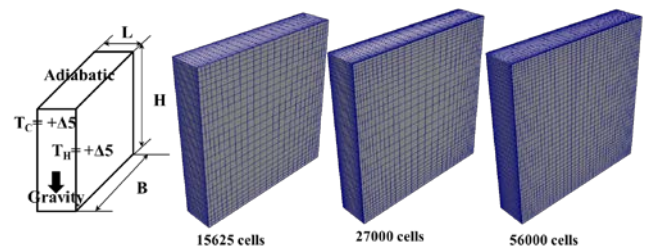
Fig. 1 Geometry and grids for validation

2.2 Validation

The pressure oscillation problem (checkerboard problem) is generally occurred in a collocated method for solving incompressible flow, and it degrades the solution or makes a calculation unstable[7, 8]. Third order diffusion term is chosen to reduce the checkerboard pressure oscillation in this study. The three-dimensional enclosed flow with natural convection has been calculated, and the results obtained from the numerical calculation for the viscous flow solver developed in this study are compared with experimental results in Ref. 9. The geometry of the three-dimensional cavity is simple and easy to handle. However, the characteristics of natural convection are nonlinear, and provide a good test of the computational procedure. The geometrical configuration and boundaries used in this study are shown in Fig. 1. The high and low temperatures are located at each side (x-direction) and the other boundaries are adiabatic. The Ra is 5×10^4 and the properties of the medium (air) are considered as constant that are listed in Table 1. To confirm Ra, density was arbitrary modified to 1.01, and the other properties are retained its origin values.

Table 1 Material property for validation

Material	Air		
		μ	1.824E-05
ρ	1.01	L	0.04
C_p	9.7703E+02	H/L	5
K	2.51 E-02	B/L	5
g	9.81	ΔT (T_h-T_c)	10
β	3.41 E-03	Pr	0.71
α	2.14E-05	Ra	5.0E+04

The velocities including computational and experimental results are plotted in Fig. 2. A good

agreement with existing experimental data [10] is obtained. The computations were performed with respect to consecutive numbers of cells (15625, 27000, and 56000). The fluid obtains heat energy from the hot wall in right side and loses it to the cold wall in left side. There is no transfer of heat energy through the adiabatic horizontal walls. It is expected that boundary layers along both hot and cold walls are exited. According to the distance between two walls, two boundary layers interfere with each other, and it may change the flow pattern and heat transfer significantly. The velocity variations between coarse and fine cells are considerably small as shown in Fig. 2. The coarse mesh can capture the characteristics of flow and temperature in the cavity properly. It implies that considering the computational cost, the small numbers of cell are sufficient for this kind of calculations.
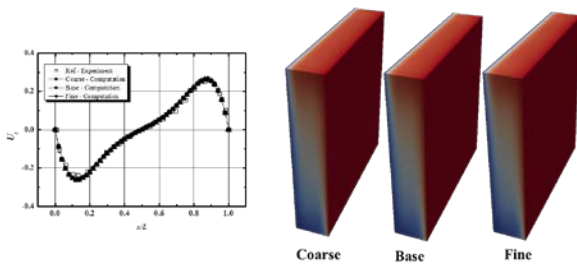
Fig.2 Velocity and temperature distributions according to the number of cells.

The flow in a three-dimensional cavity can be considered as a laminar one at Ra=5×10⁴, (viscosity effect is dominant) and develops one large vortex across the domain from top to bottom. The air next to the hot wall is heated, and moved upward along the wall by buoyancy. In despite of three-dimensional flow, an ascending air flow can be observed on the whole hot wall. On the contrary, a descending air flow can be observed on the cold wall constantly. The three-dimensional effect can be expected nearby the adiabatic walls.

3 Results and discussions

The geometry calculated in this study is the three-dimensional cavity that is similar to that of validation model except its dimensions. The height (H) and width (B) are 2m. The computation are performed with three different thicknesses (*L*=0.1, 0.15, and 0.2). The computational domain and boundaries are plotted in Fig. 3, and the specifications of the media (air) are listed in Table 2. The *Ra*s for *L*=0.1, 0.15, and 0.2 are 2.06×10^6, 6.94×10^6, and 1.64×10^7, respectively. The properties of the air are considered as constant and the

direction of the gravity is negative z-axis. It is expected that the flow make a large vortex as shown in a validation case except upper and lower dead-ends.
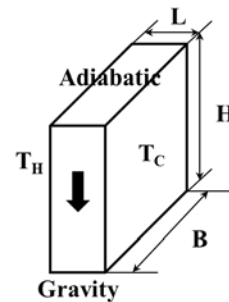
Fig. 3 Computational domain and boundaries

To decide the proper number of the cells for the calculation, the mesh dependency test for the *L*=0.1 (case01) is performed with four consecutive cells (8750, 15300, 32000, and 60750 cells). The fluxes through the cold wall are listed in Table 3. The relative error of a fine mesh shows about 0.14% against that of the finest mesh. The configurations of the fine mesh are used for the following calculation. For the convenience as shown in Table 2, the three calculations with different thicknesses such as *L*= 0.1, 0.15, and 0.2 are named "Case01, Case02, and Case03" respectively.

Table 2 Material properties and computational cases

	Case01	Case02	Case03
ρ	1.18	1.18	1.18
C_p	9.7703E+02	9.7703E+02	9.7703E+02
K	2.51 E-02	2.51 E-02	2.51 E-02
g	9.81	9.81	9.81
β	3.41 E-03	3.41 E-03	3.41 E-03
α	2.14E-05	2.14E-05	2.14E-05
μ	1.824E-05	1.824E-05	1.824E-05
L	0.1	0.15	0.20
H, B	2	2	2
ΔT	20	20	20
Pr	0.71	0.71	0.71
Ra	2.056E+06	6.939E+06	1.6448E+07

Table 3 Mesh dependency test of Case01

	No. of cells	Heat flux	Rel. error
Coarse	8750	126.37	3.65%
Base	15300	123.33	1.16%
Fine	32000	121.76	0.14%
Finest	60750	121.92	-

Table 4 Heat flux deviation according L

Cases	*L*	**Heat flux**	**Difference**
Case01	0.1	121.76	0.55%
Case02	0.15	122.26	0.13%
Case03	0.2	122.43	-
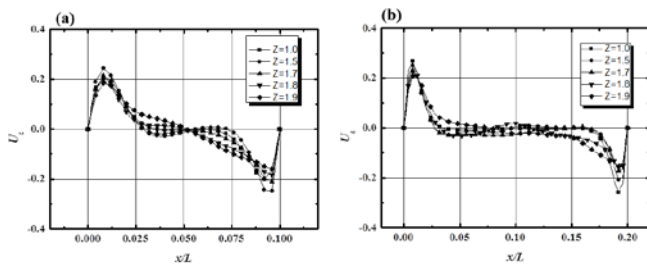
Fig. 4 Velocity distributions of Case01 and Case03.

Along the high temperature wall, the heat transfer occurs by heat conduction due to temperature difference between wall and fluid, and the fluid obtained the energy is accelerated in the opposite direction of the gravity by buoyancy effect. The buoyancy-driven flow transfers the energy to the other side of the cavity by fluid itself. During this process, the friction because of the viscosity on the wall is attended. Along the distance between two horizontal walls, the energy loss by the fluid friction increases and the velocity in the boundary layer decreases inevitably. The velocity is bound by the friction.

The flow along the high temperature wall can be divided into an acceleration region, turning-flow-direction region, deceleration region (next to beginning of low temperature wall), and acceleration region. In Fig. 4, the velocity distributions along the *x*-axis are plotted. The velocities between Case01 and the others are different each other. The maximum peak velocity of the Case01 shows at z=1.5, whereas the maximum of the Case03 does at z=1.0 since there is no interaction between two boundary layers developing from high and low temperature walls. A flat velocity area can be observed in Fig. 4(a) (z=1.0), and it implies the interaction between two layer is not severe. At above z=1.5, the velocities decrease because of upper dead-end, and gradually change its direction to the other wall. The air experiences the sudden decrease in momentum, but since the hot air having more momentum than that of low temperature air in the surrounding area; it accelerates air next to the low temperature wall. The hot air is mixed with low temperature air and lost its momentum. The cooled air moves downward and accelerated gradually along the low temperature wall. Cooled air changes its direction in the lower dead-end. It completes its vortical flow in the cavity.

In Fig. 4(a), Case01 shows more flat area (U_z~0) in the center and the variation of the velocity is lower than in fig. 4(b) for Case03. It implies that the interaction between two boundary layers in Case03

is small. The boundary layers each side develops independently and thus, the heat transfer is not changed between two layers.

As shown in Table 4, despite the increase in the thickness from **L**=0.1 to 0.2, the heat flux through the wall is constant. The deviation between Case01 and Case03 is less than 1% . In this enclosed natural convection problem, the convection heat transfer next to the wall is dominant. The air obtaining energy from the wall moves upward, and makes a boundary layer. However, the distance between two walls is sufficiently far and the interaction between boundary layers is quite small. The distance between two walls has no effect.
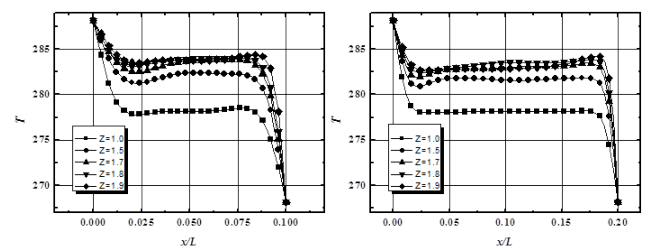
Fig. 5 temperature distributions of Case01 and Case03.

The convection heat transfer is a key of the energy transfer in this enclosed cavity. The thickness of the temperature boundary layer is thinner than that of the velocity. The flat area of the temperature is wider as shown in Fig. 5. The temperature next to the high temperature wall increases along the *z*-axis. It is expected that the energy obtained from the high temperature wall is less than energy release from the low temperature wall whereas the energy obtaining from the high temperature wall is more than energy release. In term of case01 at z>1.5, the effect of boundary interaction can be observed. Since the flow direction changes, and the temperature of the flow is still high at z>1.8, there are reverse temperature distributions. The temperature increase along the *x*-axis (right is a low temperature wall).

In Fig. 5, temperature boundary layer can be observed clearly. Both Case01 and Case03 have the same boundary layer thickness and thus, the wide float temperature can be seen in the Fig. 5(b). The temperatures increase along the *z*-axis. As shown in Fig. 5, despite of slight difference between two cases, temperature distribution next to the wall is the same and the gradients are also similar. The temperature and velocity distribution except *y*/B >0.05 are constant along *y*-axis. This implies that the flow on *z-y* plane is two-dimensional.
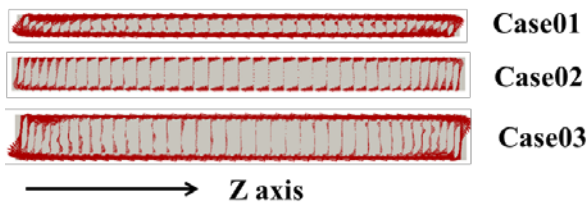
Fig. 6 Velocity vector at y=1.0
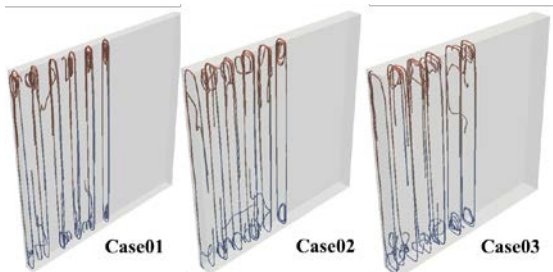
Fig. 7 Comparison of streamlines along y axis

In case of vector velocity in Fig. 6, except the upper and lower dead-end, three cases with different thickness are corresponded roughly. The only central area which has no flow increases as the width increases. The streamline in Fig. 7 shows that the major flow is vortical flow along *z*-axis and there is week secondary flow in the upper and lower dead-end.

4 Conclusion

In this study, the numerical algorithms for three-dimensional incompressible Navier-Stokes flow and energy equation on unstructured grids with arbitrary shaped cells have been developed. Third order diffusion method is employed to avoid the checkerboard pressure oscillation generally encountered in a collocated method for solving incompressible flow. Among possible energy equations, the temperature equation is used. The numerical algorithm used to solve the final linear equations is derived from the SIMPLE algorithm. The numerical methods including energy equation used have been validated with the three-dimensional cavity and a good agreement with experimental data and numerical data are obtained. Numerically, the intermediate flows until converged are complex and large fluctuation of residual can be observed.

From the flow and streamline in the cavity after fully converged, the distance between two walls (glasses) is sufficiently far and there are no boundary layer interactions. Therefore, no severe flow and temperature changes according to thicknesses are observed. A single large vortex between two walls dominates the flow and temperature characteristics. The vortex is stable, and there is no additional vortical flow between two

layers. The deviation of the temperature and flow is not severe and thus, it is note that the flow and temperature is not sensitive against thicknesses. The most of the energy transfer comes from this large vortex and the thickness has no effect on energy transfer. As a result, one large vortex approximately two-dimensional one except next to each end generated. In the near future, we perform the computation concentrating on the relations between two and three-dimensional effect according to the gap.

References:
[1] Lestari, A., *Development of Unsteady algorithms for Pressured Unstructured Solver for Two-dimensional Incompressible Flows*, Master Thesis, Iowa State University, 2009.
[2] Mathur, S.R. and Murthy, J.Y., A Pressure-based Method for Unstructured Meshes, *Numerical heat transfer, Part B*, Vol. 31, No. 2, pp. 195-215, 2007.
[3] STAR-CCM+ v402 *Methodology*, Computational dynamics Co., London 2006.
[4] Fluent ver6.2.16, *Fluent user's guide*, Lebanon, Fluent Inc. 2005.
[5] Lee, Juhee, Lee, Younjun, Flow and heat transfer of high aspect-ratio rectangular driven by natural convection, *Seoul International Conference on Engineering and Applied Sciences*, 2017.
[6] Lee, Juhee, Lee, Youngjun, *Finite Volume Method for Flow Prediction using Unstructured Meshes*, WASET, London, 2015.
[7] J. Ferziger, M. Peric, *Computational Methods for fluid for Fluid Dynamics*, 3rd Ed, Springer, Bierln, 2002.
[8] C. M. Rhie and W. L. Chow, *Numerical Study of the Turbulent Flow past and an Airfoil with Trailing Edge Separation*, AIAA J., vol. 21, pp 1525-1532, 1983.
[9] Patankar, S.V., *Numerical Heat Transfer and Fluid Flow*, Hemishpere Publishing Corp., New York, 1980.
[10] G. L. Morrison, V. Q. Tran, "Laminar flow structure in vertical free convection cavities," *Int. J. Heat Mass Transfer*, Vol. 21. pp. 203-213.